Sustainable Energy & Fuels

ROYAL SOCIETY OF CHEMISTRY

PAPER

View Article Online
View Journal | View Issue

Open Access Article. Published on 31 May 2023. Downloaded on 12/4/2025 5:24:02 PM.
This article is licensed under a Creative Commons Attribution 3.0 Unported Licence.

Check for updates

Cite this: *Sustainable Energy Fuels*, 2023, **7**, 3047

Potassium-modified bifunctional MgAl-SBA-15 for aldol condensation of furfural and acetone†

Mahashanon Arumugam, *[a] Oleg Kikhtyanin, [b] Amin Osatiashtiani, [c] Veronika Kyselová,[d] Vlastimil Fila, [e] Iva Paterova,[f] Ka-Lun Wong[gh] and David Kubička*[ab]

The aldol condensation of furfural and acetone followed by hydrodeoxygenation into bio-jet fuel range alkanes and bio-polyester diols has attracted intensive interest in recent years. Such sequential reactions require a careful tailoring of one or more catalysts consisting of metal and acid–base active sites that can efficiently promote the two step cascade aldol condensation and hydrodeoxygenation. Here, we have begun developing a prominent base catalyst for mild aldol condensation of furfural and acetone by synthesizing acid–base bifunctional MgAl-SBA-15 and further modifying it with potassium. The catalyst with the highest basic site loading of 0.27 mmol g^{-1} showed a furfural conversion of 83% and 99% total selectivity to products comprising 54% 4-(2-furyl)-4-hydroxy-butan-2-one (FAc-OH, a C_8 alcohol intermediate) and 23% of each 4-(2-furyl)-3-buten-2-one (FAc) and 1,4-pentadiene-3-one,1,5-di-2-furanyl (F_2Ac) (C_8 and C_{13} aldol condensation products, respectively) after 3 hours of reaction, at 50 °C. Though a higher loading of potassium causes severe blockages of mesopores and inaccessible acid sites, the catalyst could still be regenerated by open-air calcination and be re-used for considerable cycles with fair catalytic performances. Overall, the present study can be the stepping stone for future investigations on further tuning of non-interfering active sites in SBA-15 to promote an efficient one-pot transformation of furfural and acetone *via* the two-step cascade aldol condensation and hydrodeoxygenation.

Received 5th April 2023
Accepted 11th May 2023

DOI: 10.1039/d3se00444a

rsc.li/sustainable-energy

1 Introduction

Lignocellulosic biomass is widely regarded as one of the most sustainable, CO_2 neutral and abundant carbon sources that has evolved as an alternative feedstock in the production of renewable fuels and chemicals.[1] Acid hydrolysis of notable lignocellulosic carbohydrates like cellulose and hemicellulose can lead to hexose and pentose sugars that can be further dehydrated to a variety of potential C_2–C_6 platform chemicals such as furfural, hydroxymethylfurfural (HMF), acetone, *etc.*[2,3] Apart from ethanol and acetic acid, furfural is one of the oldest renewable chemicals, originating from non-food-based sources like agricultural waste and forest residue.[4–6] The transformation of furfural (and its derivatives) into energy-intensive fuels and chemicals *via* C–C coupling reactions, particularly aldol condensation with α-hydrogen compounds (such as ketones), followed by hydrodeoxygenation (HDO) of the aldol adducts became an area of active research in recent years. In addition, ketone, such as acetone, is produced when biomass is fermented in the Acetone–Butanol–Ethanol (ABE) process.[7] Acetone with its three-carbon molecule and carbonyl functional group, is frequently used as a substrate in aldol condensation reactions with furfural to make fuel and chemical precursors.

Aldol condensation is one of the prominent reactions in organic chemistry that has been used to produce high-quality fuels and chemical intermediates under reaction conditions (*e.g.*, 50–180 °C) with either base or acid catalysts. Conventionally, aldol condensation is catalyzed by homogeneous mineral base catalysts such as sodium and calcium hydroxide. However, the product treatment of this process requires a large amount of water to neutralize the homogeneous catalyst, which

[a]Department of Petroleum Technology and Alternative Fuels, Faculty of Environmental Technology, University of Chemistry and Technology, Prague, Technická 5, 160 00 Praha 6-Dejvice, Czechia. E-mail: arumugam@vscht.cz; kubickad@vscht.cz; Tel: +420 220 44 4237; +420 220 44 6106

[b]Technopark Kralupy VSCHT Praha, University of Chemistry and Technology Prague, nám. G. Karse 7, 278 01 Kralupy nad Vltavou, Czech Republic

[c]Energy and Bioproducts Research Institute (EBRI), College of Engineering and Physical Sciences, Aston University, Aston Triangle, Birmingham, B4 7ET, UK

[d]Department of Gaseous and Solid Fuels and Air Protection, Faculty of Environmental Technology, University of Chemistry and Technology, Prague, Technická 5, 160 00 Praha 6-Dejvice, Czechia

[e]Department of Inorganic Technology, University of Chemistry and Technology, Technická 5, 166 28 Prague 6, Czech Republic

[f]Department of Organic Technology, University of Chemistry and Technology Prague, Technická 5, 166 28 Prague, Czech Republic

[g]School of Energy and Chemical Engineering, Xiamen University Malaysia, Jalan Sunsuria, Bandar Sunsuria, 43900 Sepang, Selangor Darul Ehsan, Malaysia

[h]College of Chemistry and Chemical Engineering, Xiamen University, Xiamen, 361005, China

† Electronic supplementary information (ESI) available. See DOI: https://doi.org/10.1039/d3se00444a

Open Access Article. Published on 31 May 2023. Downloaded on 12/4/2025 5:24:02 PM. This article is licensed under a Creative Commons Attribution 3.0 Unported Licence.

has adverse effects on the environment and production cost.[8] Alternatively, solid catalysts such as MgO,[9] ZnO, and TiO_2 (ref. 10) and mixed oxides such as hydrotalcite and MgO–ZrO[8,11] have been significantly explored to replace the homogeneous catalysts. In addition, layered double hydroxides (LDHs), also known as anionic clays or hydrotalcite-like materials (HTC), have been mentioned as promising aldolization catalysts among solid base catalysts.[12–14] Moreover, re-hydrated HTC materials enable high furfural conversion in aldol condensation between furfural and acetone at temperatures as low as 25 °C.[15,16] However, several major disadvantages have been associated with these HTC materials, including high sensitivity to ambient CO_2, which makes recycling the catalysts difficult.[16–19]

Porous solid acid catalysts such as zeolites of different structural kinds, including H-ZSM-5, H-MOR, H-USY and H-BEA, have also been employed for the aldol condensation of furfural with acetone. The best catalytic behavior was observed for the H-BEA catalyst, which yielded only 30.6% FAc (furfural-acetone condensation adduct), 1.4% F_2Ac and 6.5% $(FAc)_2$ (originating from dimerization of FAc and furfural, and two FAc molecules, respectively), along with 38.5% furfural conversion at 100 °C and 2 h.[20] The lower furfural conversion is due to the kinetically slower acid-catalyzed reaction pathway, in which the activation or protonation of carbonyl oxygens of both furfural and acetone are required prior to an enol formation. This step is followed by the protonation of the hydroxyl group of a β-hydroxyketone intermediate, making it less favorable than the base-catalyzed reaction. When the reaction is base-catalyzed, a high concentration of basic sites (ideally medium-strength basic sites) is required to deprotonate the α-proton of the carbonyl compound (acetone). This results in a carbanion enolate anion formation, which is also a strong nucleophile that easily attacks the electrophilic carbonyl carbon (furfural) under mild conditions.[21]

In recent years, there has been a lot of interest in synthesizing solid mesoporous bases or employing mesoporous materials as carriers to produce basic species.[22–24] Compared to the microporous zeolites, the larger pore sizes of the mesoporous catalysts facilitate faster in-pore diffusion of bulky molecules, enabling higher accessibility to the inner catalytically active sites. Among the candidates with mesostructures, mesoporous silicas such as MCM-14 and SBA-15 seem to be the cheapest in cost and possess good hydrothermal stability.[23,25] Therefore, introducing basic guests or their precursors such as magnesium nitrate and calcium nitrate during the synthesis of SBA-15 has been one of the practicable ways of preparing a strong base.[26,27] Moreover, a superbasic mesoporous composite can be further made by dispersing neutral potassium nitrate on the directly synthesized MgO-SBA-15, followed by heat activation under an inert environment to form potassium oxide nanoparticles. The pre-coated MgO protects the mesoporous silica from the corrosion of alkaline potassium and, at the same time, improves the dispersion and decomposition of potassium salt and the formation of strongly basic sites.[27] It is important to take note that the direct contact of strong alkali metals such as potassium and caesium with the siliceous framework corrodes the siliceous framework and collapses the mesoporous structure of SBA-15 at high activation temperature, leading to the loss of the basic nature of the catalyst.[25,27] Also not long ago, Ning and co-workers constructed a new solid mesoporous superbase, comprising KF modified bimetallic Al–La supported on SBA-15 through the wetness impregnation method. The Al–La species have been conjointly precoated on the mesoporous silica surface prior to the introduction of KF salt, followed by activation at a lower temperature. The additional incorporation of Al species enhances the La dispersion inside channels, and the bimetallic species could synergistically shield SBA-15 mesoporous structures against KF corrosion, resulting in higher basicity and total surface area. Similarly, the KF modified monometallic Al supported on SBA-15 showed a well-preserved mesoporous structure, but weaker basic strength than the bimetallic Al–La doped SBA-15.

SBA-15 is an ordered mesoporous silica material that has been gaining popularity, particularly in biomass upgrading, because of the following properties: (i) high surface area for metal nanoparticles or metal-oxide dispersion,[28,29] (ii) notable thermal and hydrothermal durability,[30] (iii) large pore volumes,[31] and (iv) attractive tunable acid–base chemical characteristics.[32] These properties have also received widespread attention in the development of bifunctional acid–base SBA-15 catalysts, in which the acidic and basic active sites can be tailored on a single SBA-15 using a top-down (including post-treatment such as alumination and post-grafting of electrophilic and nucleophilic active groups)[33,34] or bottom-up (direct co-condensation of metal precursors during the synthesis stage)[35,36] approach. The post or direct grafting of SBA-15 with organic moieties, such as amino acid groups, creates acid–base bifunctional organic–inorganic hybrid mesoporous materials.[37] However, the acid–base strength of these grafted mesoporous materials is relatively weak and not as stable as metal modified materials, especially at high temperature.

The bifunctionalization of SBA-15 through *in situ* grafting of both acidic and basic sites in the mesoporous material using Mg and Al precursors has shown excellent activity and selectivity in the degradation of *N*-nitrosopyrrolidine (NPYR).[38] More recently, compartmentalization and segregation of the inorganic acidic and basic sites in hierarchical macro-mesoporous SBA-15 using a spatially orthogonal approach, along with substrate channelling, have shown improved catalytic activity in one-pot transesterification of fatty acid contaminated bio-oils and two-step cascade deacetalization-Knoevenagel condensation of dimethyl acetals to cyanates. The mesopores and macropores of the hierarchical porous framework were spatially separated with active sites, in which the mesoporous region was coated with MgO solid base nanoparticles, while the macroporous region with sulfated zirconia solid acid. Such multi- or bifunctional catalysts are essential for tandem catalytic transformation reactions.[39]

Studies of hydrodeoxygenation (HDO) of furfural–acetone aldol condensation products over SBA-15 and zeolites supported with acid and metal sites on the surface have been reported. Supported mono- and bimetallic catalysts such as Pt/Beta and Pt/Al-SBA-15, and Ni–Cu/Al-SBA-15 with a Si/Al ratio of 25 have been successfully employed for catalytic HDO of furfural-acetone adducts. The resulting products mainly contain 4-(2-furyl)-3-

Open Access Article. Published on 31 May 2023. Downloaded on 12/4/2025 5:24:02 PM. This article is licensed under a Creative Commons Attribution 3.0 Unported Licence.

buten-2-one (F-Ac) to linear C_8-alcohol. The acidic character, particularly the Brønsted acid sites created from the tetrahedral Al metal of these porous materials, promotes the hydrogenolysis of the C–O bond of the furan ring in the F-Ac molecule to diols.[40,41] Therefore, it is worthwhile to have both acid and base active sites in one single porous material, predominantly for an efficient one-pot transformation of furfural and acetone into valuable end-products like bio-jet fuel ranged alkanes and potential monomer diols that require a cascade of multiple conversion steps, including aldol condensation, hydrogenation/HDO and dehydration.

To the best of our knowledge, the basic nature of porous silica materials, particularly potassium-based promoted or modified acid–base bifunctional MgAl-SBA-15 for the aldol condensation of furfural and acetone, has not been fully explored. The Al metal has no role in the mild furfural-acetone aldol condensation reaction as the Brønsted acid sites require higher reaction temperatures, approximately 100 °C, to be active in aldol condensation.[20] Meanwhile, the Mg protects the mesoporous silica against corrosion, improves the dispersion, and facilitates the decomposition of potassium salt to form strongly basic sites. Therefore, the aim of this work is to determine the effect of the basicity of the modified bifunctional MgAl-SBA-15 on its activity and selectivity in the aldol condensation of furfural with acetone under mild reaction conditions. Besides that, the effect of the calcination environment and the method of pre-treatment of the re-used catalyst on catalytic activity has also been investigated.

2 Methodology

2.1 Preparation of *in situ* acid–base modified SBA-15

The bifunctional acid–base modified SBA-15 (x% MgAl/SBA-15) and silicious SBA-15 were prepared using a conventional liquid crystal template sol–gel synthesis method as described in the literature.[38] The x in the sample name signifies the total weight percentage of MgO and Al_2O_3 in samples, where x and the Mg/Al mol ratio were fixed at 12 and 2, respectively. Typically, 2 g of pluronic P123 (average Mn ~ 5800, Sigma) was first dissolved in a 50 mL polypropylene bottle containing 15 g of H_2O at 40 °C. 60 g of 2 M HCl (35%+, Penta Chemicals) was then added and stirred for 2 h. Prior to the addition of 4.25 g of TEOS (98%, Sigma), the gel was stirred respectively for an additional 2 h and one h after the successive addition of $Mg(CH_3COO)_2 \cdot 4H_2O$ (>98%, Sigma) and $Al(NO_3)_3 \cdot 9H_2O$ (>98%, Lach:Ner, p.a. Czech Republic) salts. The resulting gel contained TEOS: 0.02 P123: 0.16 Mg $(CH_3COO)_2$: 0.08 $Al(NO_3)_3$: 6HCl: 192H_2O. The gel mixture was then aged by stirring it at 40 °C for 24 h, and further aged at 90 °C for 48 h under an autogenous pressure and non-stirring environment. The aged gel was finally evaporated at 80 °C until the solid sample was recovered and calcined at 550 °C (ramped at 1 °C min^{-1}) for 5 h.

2.2 Preparation of K_2O promoted acid–base SBA-15

The stronger basic catalyst was prepared by dry impregnation of different amounts (y wt%) of KNO_3 salt (>98%, Lach: Ner, p.a.) with the above modified SBA-15 according to the procedure reported by Zheng *et al.*[27] The mixed solid mixture was wetted into a paste with a small amount of water, approximately 65% more than the total weight of prepared catalysts, and ground for 10 min. It was then dried overnight in an oven at 110 °C. The mass of water used was varied according to the densities of the acid–base modified SBA-15, which were five to six times more the total weight of the modified SBA-15. The sample was ground again for 10 min before being dried overnight in the oven at 110 °C. The sample was then calcined under a flow of 30 mL min^{-1} N_2 at 550 °C with a ramp rate of 3 °C min^{-1} and held for 2 h. The final sample is denoted as $y$$K_2O$/12MgAl/SBA-15, where y denotes the weight percentage of the KNO_3 coated on the modified SBA-15.

2.3 Preparation of MgAl layered doubled hydroxide (LDH)

In this study, MgAl layered doubled hydroxide (LDH) with a Mg/Al molar ratio of 2 was chosen as a benchmark catalyst for the aldol condensation. The MgAl LDH was prepared using a co-precipitation technique adapted from our previous work.[15] Typically, an aqueous solution containing $Mg(NO_3)_2 \cdot 6H_2O$ (99.9%, Lach:Ner) and $Al(NO_3)_3 \cdot 9H_2O$ (98.8%, Lach:Ner) with a 0.5 mol L^{-1} concentration of total metal ions was slowly added to 200 mL of double-distilled water. Subsequently, alkaline solutions of Na_2CO_3 (0.2 mol L^{-1}) (99%, Penta) and NaOH (1 mol L^{-1}) (99.6%, Lach:Ner) were added simultaneously at a flow rate that maintains the reaction pH at the desired value of 10.0 ± 0.1. The co-precipitation was carried out at 25 °C and 400 rpm. The final suspension was then aged at 25 °C for 1.5 h under constant stirring. The product was filtered out, rinsed with distilled water, dried overnight at 60 °C, and then calcined at 400 °C with a ramp rate of 3 °C min^{-1} for 4 h. After calcination, the catalyst was sealed in a glass vial and then stored in a desiccator before the catalytic testing. Following that, z wt% of KNO_3 promoted 2MgAl was prepared according to the method described in Section 2.2, where z denotes the weight percentage of KNO_3 coated on the 2MgAl. The catalytic test was performed on the same day to prevent the basic catalyst from reacting with CO_2 from the surrounding environment.

2.4 Characterization

Nitrogen porosimetry was performed on a 3Flex analyzer, Micromeritics, Norcross, USA. The samples were degassed at 150 °C for 12 h in a vacuum prior to the N_2 adsorption analysis at −196 °C. The specific surface area was determined using the Brunauer–Emmett–Teller (BET) method within the relative pressure range of 0.02–0.2. The microporosity present was determined using t-plot analysis over the relative pressure range of 0.2–0.5. The DFT method was used for determining the pore size distribution.

Low angle XRD was performed in the range of $2\theta = 0.5$–$10.0°$ with a step size of 0.01° and a scan step of 0.6 s using a Bruker – D8 Advance diffractometer UK, fitted with an X'celerator detector with Co Kα ($\lambda = 1.54$ Å). The wide angle XRD patterns were recorded in the range of $2\theta = 10$–$80°$ with a step size of 0.03° and scan rate of 1.0 s using a PANalytical X'Pert3

Open Access Article. Published on 31 May 2023. Downloaded on 12/4/2025 5:24:02 PM. This article is licensed under a Creative Commons Attribution 3.0 Unported Licence.

diffractometer and Cu Kα (λ = 1.78 Å). An ARL 9400, Axios, PERFORM'X XRF was used to determine the elemental composition of the bulk catalysts.

An EFTEM Jeol 2200 FS, Japan, with an accelerating voltage of 200 kV was used to investigate the morphology of the calcined catalysts. The surface composition of the catalyst was determined by mapping technique using an EDX from AZtec Oxford Instruments.

CO_2-TPD was measured using an AutoChem II 2920 (Micromeritics Instrument Corp., USA) equipped simultaneously with a TCD and an MS (Pfeiffer Omnistar GSD320, Germany) detector. About 60 mg of calcined samples were initially pretreated in a helium atmosphere at 550 °C to remove surface moisture and impurities. The samples were cooled down to 50 °C prior to adsorption with a CO_2 molecule for 30 min, followed by purging out any excess pyridine and CO_2 with helium (25 mL min^{-1}) at 50 °C. The desorption of CO_2 was performed by heating the samples from 50 °C to 800 °C at a heating rate of 10 °C min^{-1} under a 25 mL min^{-1} flow of He and held for 30 min. The CO_2-TPD profile was recorded as relative mass 44/4 (CO_2) by using a MS detector using m/z signal 44, which was divided by the signal of the carrier gas He to achieve higher precision.

The acid site loading was determined using temperature programmed decomposition of *n*-propylamine to propene and NH_3 *via* the Hoffman elimination reaction principle.[42] About 10 mg of sample was wetted with 0.4 mL of *n*-propylamine and dried in a fume hood at room temperature. The physisorbed *n*-propylamine was subsequently evaporated in a vacuum oven overnight at 40 °C and 100 mbar. The *n*-propylamine treated samples were analysed with thermogravimetric analysis (TGA) using Setaram SETSYS Evolution TGA-DTA Thermal Analyzer (Caluire, France) instrument equipped with mass spectrometer Pfeiffer Omnistar GSD 320 from 50 to 800 °C with a ramp rate 10 °C min^{-1} under a N_2 atmosphere (30 mL min^{-1}). The m/z = 41 signal for propene was monitored to determine the temperature range over which *n*-propylamine decomposed and the corresponding mass loss over this range in TGA was used to calculate the moles of *n*-propylamine adsorbed at acid sites.

The thermogravimetric-differential thermogravimetric (TGA-DTG) analysis of the regenerated catalyst was performed using a TA Instruments TGA Discovery series equipment, USA. The catalyst was heated from 50 to 900 °C with a heating rate of 10 °C min^{-1} and an O_2 flow of 30 mL min^{-1}.

2.5 Catalytic test

As reported in our previous method,[12] furfural (99%, Sigma) was distilled, stabilized with 2,6-di-*tert*-butyl-4-methylphenol (BHT, 99%, Sigma-Aldrich), and stored in an amber bottle, chilled before all catalytic experiments. The furfural was initially distilled to remove the acid impurities, which were originally present in the as-obtained furfural using a rotary evaporator at around 130 °C with a vacuum pressure close to −0.8 bar. The distilled furfural was then mixed with a stabilizer at a weight ratio of 375 parts furfural to 1 part stabilizer. The total acid content of the furfural was determined by titrating against 0.01 M potassium hydroxide using a Karl Fischer auto-titrator model 716 DMS Titrino (Herisau, Switzerland). The acidity of distilled furfural used in this study was 0.0031 mmol equivalents of acids present per gram of furfural. Aldol condensation was performed using 3.25 g furfural and 12.5 mL acetone with a molar ratio of (1 : 5) in a 50 mL glass flask reactor. The mixture was preheated at 50 °C before adding 0.25 g of catalyst. The aldol condensation experiments were carried out at 50 °C (±1 °C) under a stirring rate of 300 rpm. About 0.1 mL of samples were intermittently withdrawn from the reaction mixture, filtered through a 0.45 μm PTFE filter and diluted in methanol before being analyzed with an Agilent 7890A gas chromatograph equipped with a flame ionization detector (FID), and an HP-5 capillary column (30 m length, 0.32 mm ID, 0.25 μm thickness). The catalytic performance in the aldol condensation was expressed as conversion and selectivity.

Furfural conversion was calculated based on the formula: $x\ (\text{mol\%}) = \dfrac{x_0 - x_t}{x_0} \times 100\%$ where: x_0 is the initial mol of furfural at time 0 min and x_t is the mol of furfural at time, t.

Product selectivity was calculated as follows: $S\ (\%) = \dfrac{n_x = i}{\Sigma_{n_x}} \times 100\ \%$ where: n_x is the moles of furfural converted to product i and Σ_{n_x} is the total moles of furfural converted.

All the catalytic experiments were performed in duplicate or triplicate with comparable data, and the experimental errors were within ±5%. Carbon balance was calculated by dividing the total number of carbon atoms detected in each compound produced with C_n atoms (n = 3, 5, 8, 13 *etc.*) by the initial number of carbon atoms in the feedstock containing furfural and acetone. In all experiments, the carbon balance was very close to 100%.

3 Results and discussion

3.1 Characterization

Elemental analysis and physicochemical properties of the prepared catalysts are shown in Tables 1, S1, 2 and S2.† XRF analysis reveals the existence of all the major oxides in the samples, and the experimental compositions are closely matched to their respective theoretical values. Fig. 1a and b exhibit low and wide-angle XRD diffractograms of SBA-15 samples. The acid–base modified samples show well-resolved diffraction peaks with a prominent long-range ordered mesopore peak below $2\theta = 1.0°$, along with weak peaks at 1.6° and 1.9°, which can be assigned to the diffraction planes of (100), (110) and (200). These diffraction planes are typical of 2D hexagonal pore ordering of the *p6mm* space group reported for SBA-15 previously. As highlighted in the literature,[38] the direct incorporation of Mg and Al has made the diffraction planes more intense than the parent SBA-15, elucidating that the metal salts improved the ordered mesostructure of SBA-15.[43] Further incorporation of K salt from 8 to 20 wt% onto the samples has drastically weakened the peak intensities of SBA-15, mainly due to the pore blockages. No diffraction peaks due to the crystalline phase of MgO, Al_2O_3 or K_2O are observed from the

Open Access Article. Published on 31 May 2023. Downloaded on 12/4/2025 5:24:02 PM. This article is licensed under a Creative Commons Attribution 3.0 Unported Licence.

Table 1 Elemental composition[a]

Parameter/sample	Unit	SBA-15	12MgAl-SBA-15	$8K_2O$/12MgAl-SBA-15	$20K_2O$/12MgAl-SBA-15
SiO_2	wt%	99.53	86.03	77.97	66.11
Al_2O_3	wt%	—	4.86	5.11	4.17
MgO	wt%	—	8.42	8.29	7.14
K_2O	wt%	0.12	0.10	8.19	21.43
Other impurities[b]	wt%	0.35	0.59	0.44	1.15
Si/Al	mol mol^{-1}	—	15.1	13.0	15.9

[a] Determined by XRF analysis. [b] Impurities including Cl, SO_3, P_2O_5, CaO, Na_2O, CuO, ZnO and Fe_2O_3.

wide angle XRD patterns, indicating that the oxides formed on SBA-15 are either well dispersed or have particle size in the low nanometre range. Likewise, TEM analysis shows that the addition of metal precursors does not influence the morphology of the SBA-15 composite significantly (Fig. 2). The modified samples displayed ordered one-dimensional straight channels and retained the same hexagonal mesostructure as the parent SBA-15. The elemental mapping images show a homogeneous dispersion and interaction of guest particles with the silica framework throughout the SBA-15 composite. The XRF analysis of the 2MgAl mixed oxide counterpart demonstrates that the synthesized material has the same Mg/Al mol ratio (~2) as the theoretical one (Table S1†). The XRD pattern of the calcined 2MgAl shows that only the MgO crystalline phase is present, as evidenced at $2\theta \approx 43.0°$ and 62.5° (Fig. S1†). When KNO_3 is introduced, new diffraction peaks can be observed at 27.35°, 29.72°, 32.84°, 39.41°, 44.43° and 44.85°, referring mainly to the planes of rhombohedral KNO_3 (JSPDS no: 01-078-7937). The presence of a small amount of K_2O is observed with the peaks centred at 27.35°, 39.41°, 43.26°, 62.77° and 76.60° (JSPDS no: 01-089-3998). The diffraction peaks of K_2O mostly overlap with those of KNO_3. The significant phase composition of KNO_3 could be due to the lower calcination or activation temperature (550 °C) that did not totally decompose all the KNO_3 salt to K_2O.[27]

In accordance with IUPAC classification for mesoporous materials, both parent and modified SBA-15 possess typical type IV isotherms (Fig. S2†), with the BET surface area decreasing with the metal incorporation. As the concentration of guest species added to the parent SBA-15 increases, the BET surface areas and total pore volumes drastically reduce to 94% and 80%. The pore size distribution of SBA-15 samples before and after bifunctionalization is shown in Fig. 1b. DFT pore size measurement indicates that the pore width of the parent SBA-15 lies between 1.6 and 2.4 nm and 6.6 and 9.3 nm, corresponding to micro- and meso-pore sizes of typical SBA-15. The pore size distribution of the modified SBA-15 sample is more constrained, lying only in the mesopore range of 6.5–9.7 nm than the parent SBA-15. However, when the K_2O content reaches 20%, the pore size of the modified SBA-15 completely disappears compared to that of the host, suggesting a high degree of pore obstruction.[44]

Fig. 3a depicts a small peak centered at 110 °C that appeared on the bare SBA-15 support due to the release of weakly adsorbed CO_2 from the SBA-15 surface during CO_2-TPD analysis.[27] *In situ* bifunctionalization of 12 wt% Mg and Al on SBA-15 does not form any new basic sites, as the desorption of CO_2 remains in the weak basic site region (<200 °C) with a maximum temperature T_{max} of 118 °C and total basic sites of 0.007 mmol g^{-1}. Further incorporation of 8 and 20 wt% K_2O species leads to the appearance of new CO_2 desorption peaks at a T_{max} of 492 and 653 °C, demonstrating a close association between the intense increase in basicity and the K_2O species. In addition, the total basic site loading of the 20 wt% K_2O loaded catalyst (0.236 mmol g^{-1}) is 35 times more than that of 12MgAl-SBA-15 (0.007 mmol g^{-1}). The excess strong basic sites are attributed to highly dispersed KNO_3 salt on the Mg coated-SBA-15, followed

Table 2 Physicochemical properties

	Base and acid site loading									
Catalyst	T_{max} (°C)	Basic site loading[a] (mmol g^{-1})	T_{max} (°C)	Acid site loading[b] (mmol g^{-1})	S_{BET}[c] (m^2 g^{-1})	S_{MIC}[d] (m^2 g^{-1})	S_{EXT}[e] (m^2 g^{-1})	V_p[f] (cm^3 g^{-1})	V_{mic}[d] (cm^3 g^{-1})	V_{mes}[g] (cm^3 g^{-1})
$20KNO_3$/12MgAl-SBA-15	168, 616	0.276	—	—	—	—	—	—	—	—
$20K_2O$/12MgAl-SBA-15	172, 653	0.236	418	0.050	30	0	30	0.21	0.00	0.21
$8K_2O$/12MgAl-SBA-15	109, 492	0.029	361, 502	0.040	261	12	249	0.66	0.01	0.66
12MgAl-SBA-15	115	0.007	426	0.470	485	31	454	0.92	0.02	0.91
SBA-15	108	0.006	154	0.290	531	54	477	0.98	0.02	0.96

[a] From CO_2-TPD. [b] From propylamine-TGA-MS. [c] S_{BET} total surface area determined using the BET equation with $P/P_0 < 0.05$. [d] S_{MIC} micropore surface area and V_{MIC} micropore volume determined from *t*-plot analysis. [e] S_{EXT} external surface area was calculated from the difference between S_{BET} and S_{MIC}. [f] V_p total pore volume obtained from the isotherm at $P/P_0 = 0.99$ (error = ±10%). [g] V_{MES} mesopore volume obtained from the difference between V_p and V_{MIC}.

Open Access Article. Published on 31 May 2023. Downloaded on 12/4/2025 5:24:02 PM.
This article is licensed under a Creative Commons Attribution 3.0 Unported Licence.

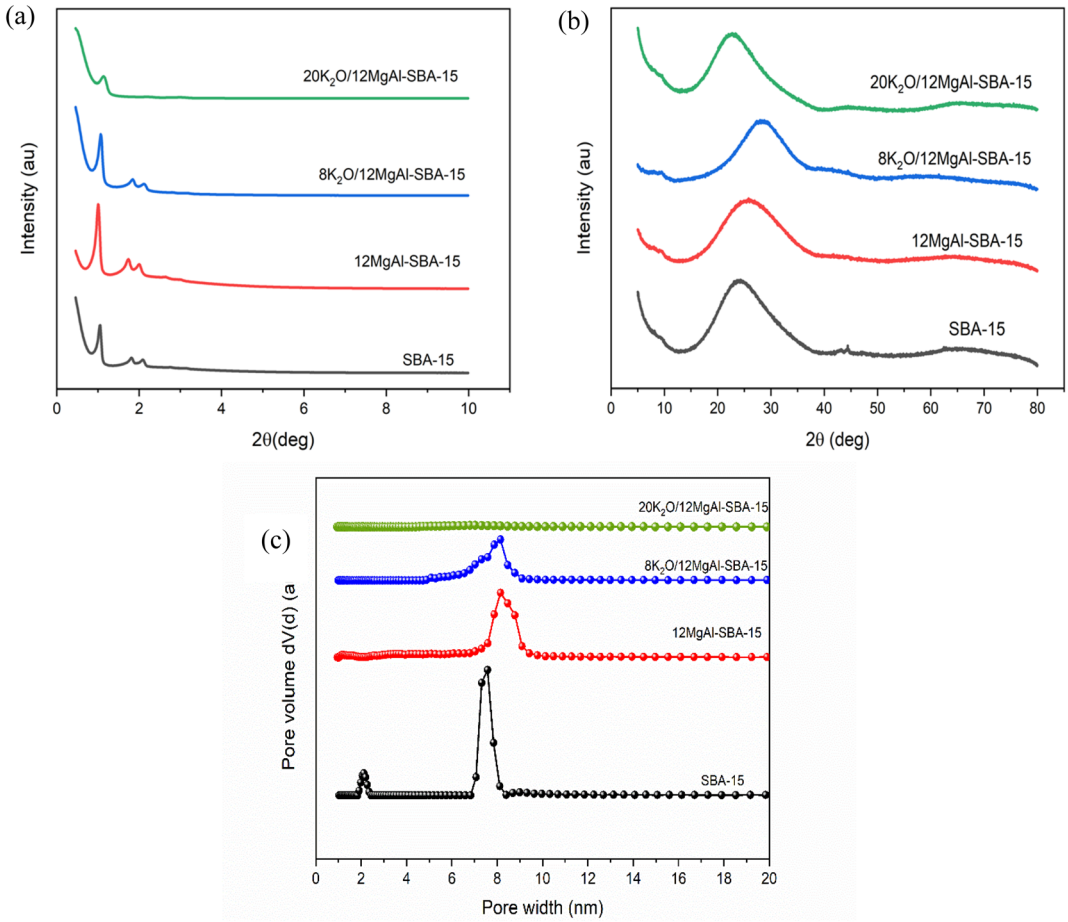

Fig. 1 (a) Low angle and (b) wide angle XRD patterns, and (c) DFT pore size distribution for parent SBA-15 and modified SBA-15 catalysts.

by its decomposition to K_2O by thermal treatment under a N_2 environment. As a comparison, the CO_2-TPD analysis was also performed on a non-calcined $20KNO_3$/12MgAl-SBA-15 sample, which exhibited fifteen times more basic site loading (0.276 mmol g^{-1}) and a comparable basic site strength of T_{max} = 616 °C to $8K_2O$/12MgAl-SBA-15. Apart from $20KNO_3$/12MgAl-SBA-15, all the samples were pre-calcined and subsequently activated at 550 °C for 2 h under N_2 prior to CO_2 adsorption before the CO_2-TPD analysis. However, we speculate that due to high sensitivity towards CO_2 and poor activation temperature, the pre-calcined samples possess poor basic sites in comparison with the freshly prepared non-calcined sample. It is evident from the temperature-programmed decomposition (TPDE) analysis that the KNO_3 salt on the MgO-modified SBA-15 completely decomposes after activation at 600 °C.[27] Concerning the CO_2-TPD result of HTC material (Table S1 and Fig. S3a†), a higher basic strength is observed at T_{max} 404 °C and 642 °C, in conjunction with the potassium incorporation onto 2MgAl. Compared to 2MgAl, higher basic site loadings of 0.38 and 0.11 mmol g^{-1} are exhibited by $20K_2O$/2MgAl at T_{max} 404 °C and 642 °C. In contrast, 2MgAl shows basic site loadings of 0.53 and 0.04 mmol g^{-1} at a T_{max} of 230 °C and 648 °C, respectively.

The mass spectra of reactively formed propene (m/z = 41) and the corresponding desorption temperature of the chemisorbed *n*-propylamine are shown in Fig. 3b. Usually, the decomposition temperature of adsorbed isopropylamine to propene and ammonia occurs between 300 °C and 550 °C.[45] In this study, the parent and modified SBA-15 showed a low-temperature desorption peak of propene below 200 °C, which can be ascribed to physisorbed propylamine. The presence of strong acid sites on modified 12MgAl-SBA-15 is evidenced by a larger high-temperature desorption peak that appeared at a maximum temperature of 426 °C, with an acid site loading of 0.47 mmol g^{-1} that can be associated with the release of propene from strong acid sites. The incorporation of 8 wt% potassium on the modified-SBA-15 has reduced the catalyst's acidity drastically by 12 times, due to the obstruction of Brønsted acid sites (Si–OH–Al) by the potassium particles. As for the HTC material, the acid site loading of $20K_2O$/2MgAl was ~60% lower than that of unmodified 2MgAl (Fig. S3b†), with a slight shift to a lower decomposition T_{max} of 295 °C. The lower decomposition temperature indicates blockages of Lewis acid sites of 2MgAl after the high potassium loading.

3.2 Catalytic part

In this work, the furfural-acetone aldol condensation was performed using a glass batch reactor with a fixed molar ratio of 1 : 5 of furfural and acetone and a constant temperature of 50 °C

Open Access Article. Published on 31 May 2023. Downloaded on 12/4/2025 5:24:02 PM.
This article is licensed under a Creative Commons Attribution 3.0 Unported Licence.

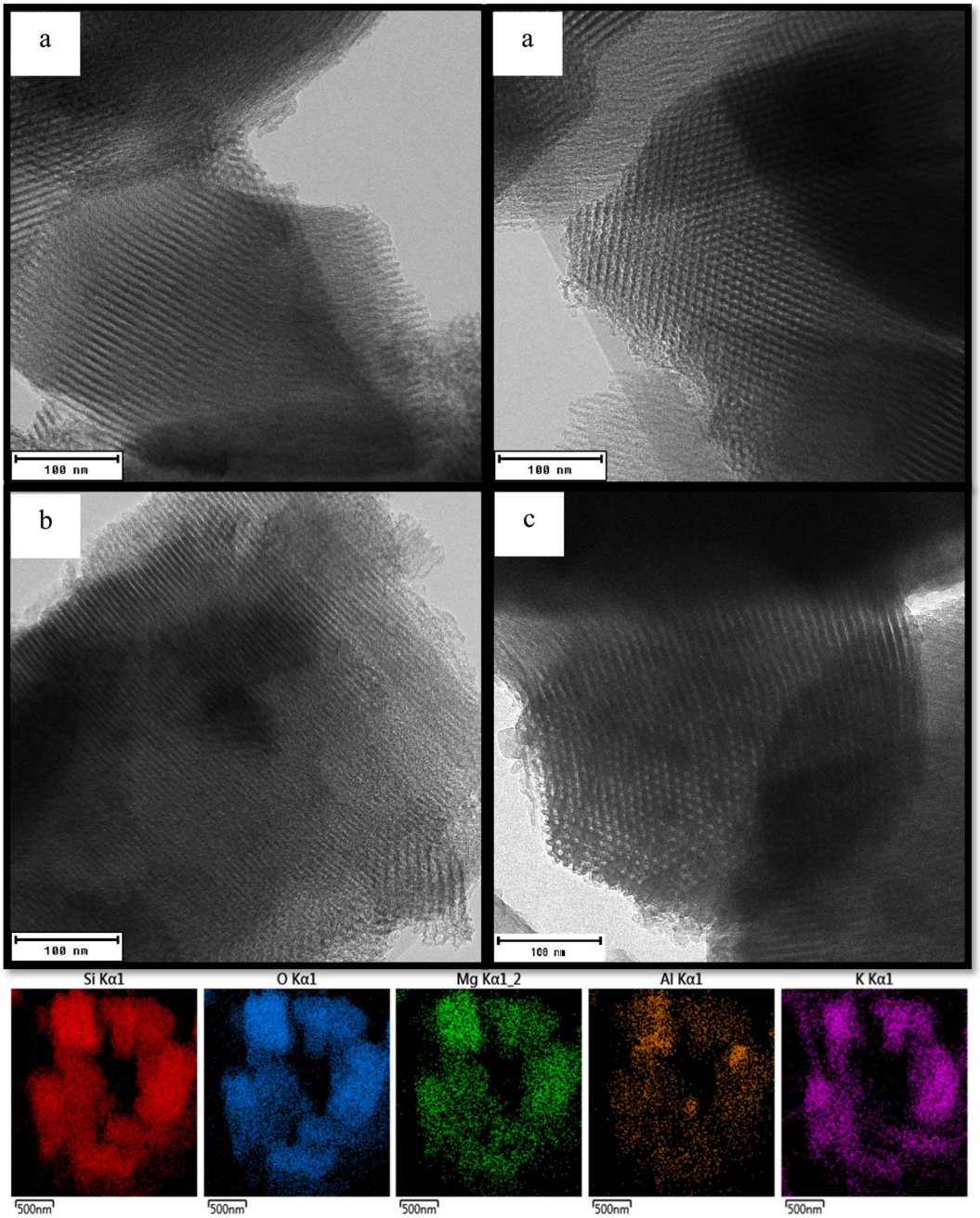

Fig. 2 TEM images for (a) SBA-15 (b) 12-MgAl-SBA-15 and (c) 20K_2O/12MgAl-SBA-15 and elemental mapping of 20K_2O/12MgAl-SBA-15.

throughout all the experiments. The products of the furfural-acetone aldol condensation are depicted in Scheme 1. The bifunctional 12MgAl-SBA-15 and potassium-incorporated catalysts were prepared under open-air and N_2 environment calcinations and kept in a desiccator prior to the catalytic study. The effect of basic sites on furfural conversion and selectivity is shown in Fig. 4. Of all the tested catalysts, the acid–base bifunctional 12MgAl-SBA-15 shows no activity for the aldol condensation, plausibly due to the small number of basic sites. However, an increase in the basic site loading of the bifunctional catalyst significantly improved the progression of furfural conversion. As foreseen, a higher conversion of furfural was achieved with increasing potassium content. Fig. 4(b–d) also reveal that at a low iso-conversion of 10–20%, when the catalyst deactivation is minimal, the selectivity to FAc-OH drops marginally, but selectivity to F_2Ac rises with increasing basicity. This phenomenon is explained by the fact that the strongly basic sites in $x$$K_2O$/12MgAl-SBA-15 contribute more to the overall performance of the catalyst, especially the second aldol condensation step of FAc to F_2Ac. In the case of the HTC catalyst (Fig. S4a–c†), introducing 20 wt% potassium into the 2MgAl HTC catalyst doubled its catalytic activity compared to unmodified 2MgAl, achieving furfural conversions of 40% and 91% with 3 h and 24 h reaction times. It is apparent that the

Open Access Article. Published on 31 May 2023. Downloaded on 12/4/2025 5:24:02 PM.
This article is licensed under a Creative Commons Attribution 3.0 Unported Licence.

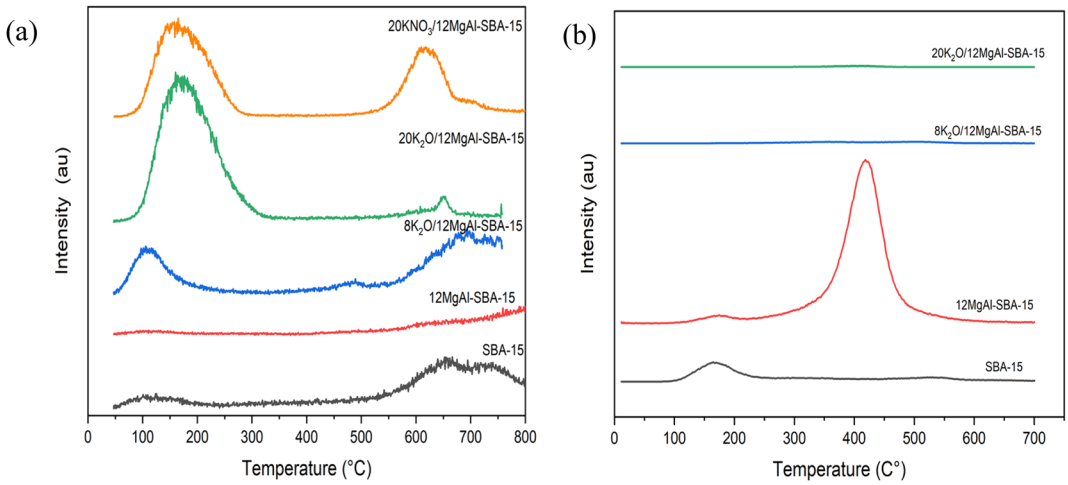

Fig. 3 (a) CO_2-TPD and (b) TGA-MS-propylamine of parent and modified SBA-15.

catalytic activity of the potassium promoted 2MgAl is in good agreement with the basic strength of the catalyst as depicted in its CO_2-TPD experiment.[46] Meanwhile, the selectivity result of $20K_2O$/2MgAl shows that FAc and F_2Ac concentrations increased dramatically to 46% and 32% with furfural conversion, indicating a faster dehydration rate of the FAc-OH intermediate over the strongly basic sites of the catalyst. However, although $20K_2O$/2MgAl has higher basic site strength and loading and a comparable BET surface area, a furfural conversion of only 65% has been achieved within 3 h reaction time compared to its counterpart, $20K_2O$/12MgAl-SBA-15. This anomaly could be due to the better dispersion and decomposition of the potassium salt on the mesostructured SBA-15,[27] particularly, the bifunctional 12MgAl-SBA-15 which has a higher surface area and porosity than the mixed metal oxide 2MgAl.

Based on the catalytic results from the previous section, it can be concluded that K_2O doped onto the acid–base bifunctional 12MgAl-SBA-15 has stronger basic sites and thus, exhibited superior catalytic activity for the furfural and acetone aldol condensation under mild conditions of 50 °C. This is because of the strong interaction between potassium and precoated Mg on SBA-15 that promotes the dispersion and decomposition of KNO_3 salt into K_2O, thereby creating a strongly basic site in the catalyst. However, metal species incorporated on materials such as oxides, zeolites, and SBA-15 *via* preparation techniques such as impregnation and co-precipitation can be unstable and slowly leach out into the reaction mixture over time. As a result, the reusability of the spent $20K_2O$/12MgAl-SBA-15 was evaluated to assess its stability and robustness in the aldol condensation reaction.

Fig. 5a and b show the catalytic activities of the re-used and regenerated $20K_2O$/12MgAl-SBA-15 with different methods and repeated open-air calcination. Initially, the used catalyst was regenerated by thermal treatment under an N_2 atmosphere at 550 °C for 2 h. The catalyst, however, was completely deactivated, mainly due to the incomplete oxidation of the aldol adduct residue. The incomplete oxidation of the aldol adduct residue in the N_2 environment was proven with the TGA experiment, in which it degraded from 250 to 500 °C (Fig. S5†).[47,48] When the calcination is performed under N_2, the residue adsorbed on the catalyst's surface turns into carbon, thus blocking its active site. For this reason, after the first catalytic run, the spent catalyst was recycled by rinsing with acetone several times and drying overnight at 110 °C. However,

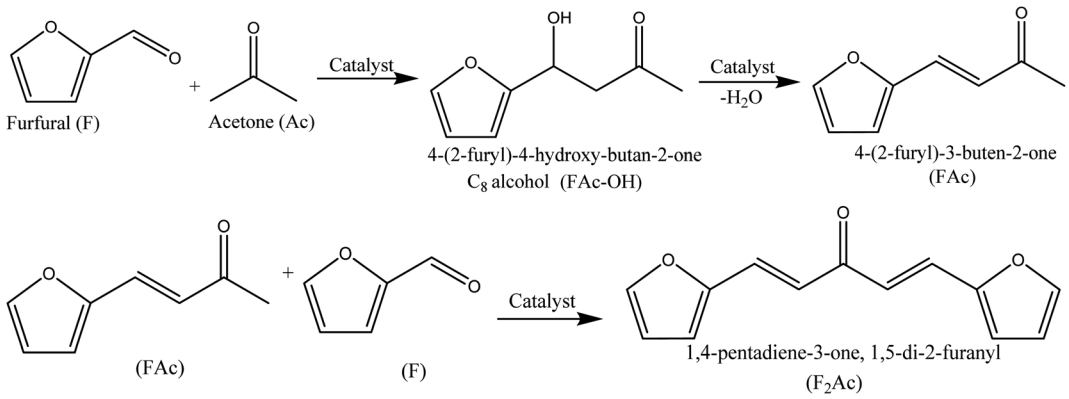

Scheme 1 Reaction scheme of the furfural and acetone aldol condensation.

Open Access Article. Published on 31 May 2023. Downloaded on 12/4/2025 5:24:02 PM.
This article is licensed under a Creative Commons Attribution 3.0 Unported Licence.

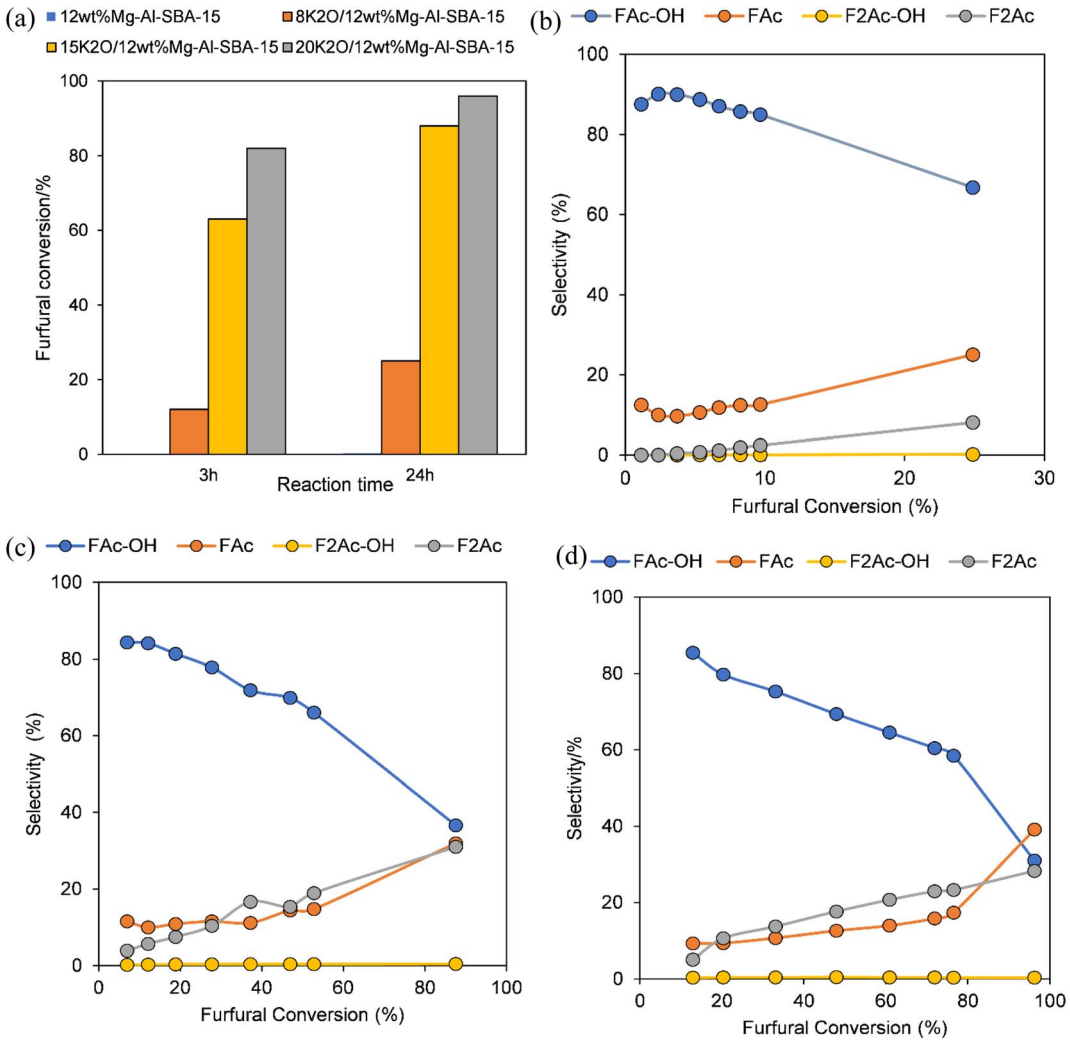

Fig. 4 (a) Comparison of furfural conversion and (b–d) product selectivity as a function of furfural conversion achieved over 24 h using different concentrations (8, 15 and 20 wt%) of potassium modified 12MgAl-SBA-15.

the catalytic performance of the recycled catalyst was significantly reduced, with furfural conversion decreasing to 31% after a reaction time of 24 h. Following the poor catalytic performance, the spent catalyst from the second run was filtered and cleaned with a Soxhlet extractor using ethyl acetate for 24 h at an extraction temperature of 100 °C and replaced with acetone for 8 h. The recycled catalyst, nevertheless, showed no improvement in the activity and instead suffered serious deactivation, with furfural conversion reaching only 0.3% after 24 h. The result implies that the $20K_2O/12MgAl$ catalyst cannot be recycled through washing with acetone and Soxhlet extraction alone after the reaction.

A further attempt to revive the catalyst performance was continued by filtering out the spent catalyst and washing it with acetone and finally regenerating it thermally by open-air calcination at 550 °C for 2 h. After 24 h of reaction, the catalytic behaviour of the regenerated catalyst was restored but only up to 15%. This suggests that the restoration of catalytic activity can be fixed by burning off the carbon residue and aldol adducts adsorbed on the catalyst's surface. Subsequently, the furfural-acetone aldol condensation reaction was re-investigated using potassium nitrate incorporated on 12MgAl-SBA-15 that was freshly prepared and regenerated using open-air calcination instead of a N_2 atmosphere. 20 wt% potassium incorporated on the acid–base modified 12MgAl-SBA-15 was calcined in air at 550 °C for 2 h, and the catalyst was removed from the furnace at around 400 °C, sealed in a glass vial, and then stored in a desiccator prior to the aldol condensation experiment. The catalytic test was performed on the same day to avoid contamination of CO_2 from the atmosphere. The fresh $20K_2O/12MgAl$-SBA-15 displayed a slightly lower furfural conversion of 65% after a reaction time of 24 h than the catalyst prepared under the N_2 environment. As expected, the decrease in the activity indicates the high sensitivity character of the strongly basic material (combination of K_2O and MgO) towards ambient CO_2.[27] The $20K_2O/12MgAl$-SBA-15 catalyst from run one was regenerated by acetone washing, followed by drying and calcination in open-air (the same conditions for run 1), and successively tested in the next run 2. The same regeneration step was repeated in subsequent runs 3 and 4. The catalytic

Open Access Article. Published on 31 May 2023. Downloaded on 12/4/2025 5:24:02 PM.
This article is licensed under a Creative Commons Attribution 3.0 Unported Licence.

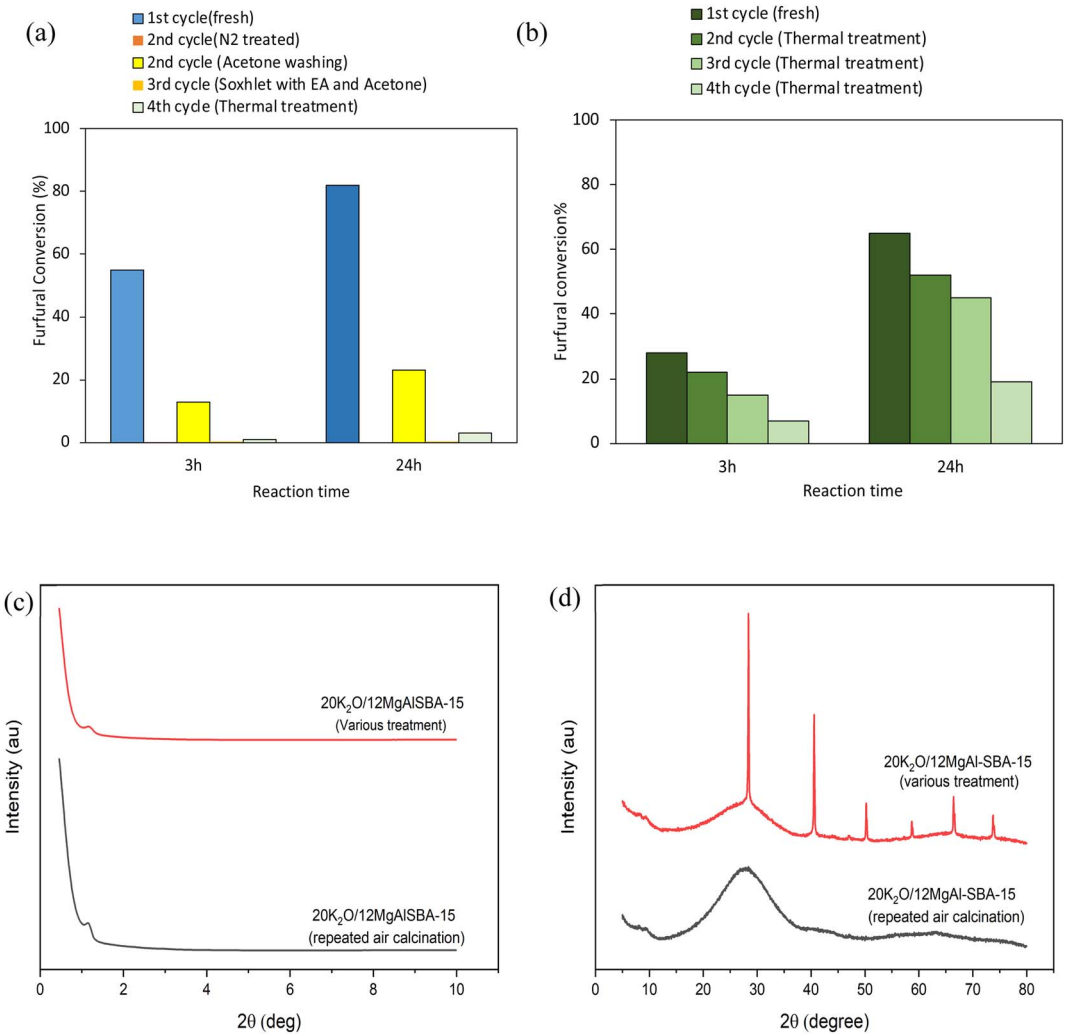

Fig. 5 Reusability performance of the re-used $20K_2O/12MgAl$-SBA-15 over four reaction cycles with (a) four different treatments, including calcination under a N_2 environment, acetone washing and drying, cleaning with Soxhlet apparatus using ethyl acetate (EA), followed by acetone washing and open-air calcination, and (b) four consecutive open-air calcinations; (c) low-angle, and (d) wide angle XRD of the calcined catalysts regenerated after the fourth cycle.

performance of the regenerated catalyst decreased slightly in runs 2 and 3, with a furfural conversion of 52% and 45%, but very dramatically to 15% in run 4.

An investigation on the cause of the catalyst deactivation in reusability experiments was carried out by recovering the spent catalysts after run 4 and cleaning them with acetone, followed by

Table 3 Elemental composition[a] of the regenerated $20K_2O/12MgAl$-SBA-15 catalysts after the fourth reaction[b]

Parameter/sample	Unit	$20K_2O/12MgAl$-SBA-15 (various treatment)[c]	$20K_2O/12MgAl$-SBA-15 (repeated air calcination)
SiO_2	wt%	65.29	70.18
Al_2O_3	wt%	4.21	4.73
MgO	wt%	7.04	8.05
K_2O	wt%	17.43	15.39
C1	wt%	4.03	0.15
Other impurities[d]	wt%	2.00	1.50
Si/Al	mol mol^{-1}	13.2	12.6

[a] Determined by XRF analysis. [b] The regenerated $20K_2O/12MgAl$-SBA-15 catalysts reported in the table refer to the same re-used catalyst shown in Fig. 5(a) and (b) regenerated after the fourth aldol condensation reaction. [c] The various treatments refer to the treatments shown for the Fig. 5(a) re-used catalyst. [d] Impurities including Cl, SO_3, P_2O_5, CaO, Na_2O, CuO, ZnO and Fe_2O_3.

Open Access Article. Published on 31 May 2023. Downloaded on 12/4/2025 5:24:02 PM. This article is licensed under a Creative Commons Attribution 3.0 Unported Licence.

calcining in air, and then characterizing them with structural and elemental analyses. Fig. 5c and d, and Table 3 show the results of the XRD and XRF analyses of the regenerated catalysts from both reusability experiments. The low-angle XRD of the regenerated catalysts shows a slight shift in a diffraction plane (1 0 0) to a higher angle value of 1.25° compared to the freshly prepared catalyst in Fig. 1a. The shift in the diffraction angle could be due to the contraction of the silica frameworks after a repeated number of calcinations.[49] The low intensity of the 1.25° peak, relative to those shown in Fig. 1, indicates that the mesoporous structure has been greatly blocked. Meanwhile, the wide-angle XRD results for spent catalysts from various treatments were contradictory to those of the fresh catalysts as the diffraction peaks for potassium chloride were observed at 2θ values of 28.37°, 40.55°, 50.22°, 58.68°, 66.43° and 73.74°. It can be anticipated that the various physical treatments of the spent catalyst could have led to the formation of crystalline potassium compounds on the catalyst surface, thus resulting in inferior catalytic performance. Compared to the fresh catalyst, XRF results indicate a 19 wt% and 28 wt% loss in the potassium content with respect to the catalyst regenerated after various treatments and continuous open-air calcination. The loss of potassium metal in the catalyst could be the primary reason, resulting in a loss of the catalytic activity for the aldol condensation of furfural and acetone.

4 Conclusions

To the best of our knowledge, our study is the first to explore the effect of the basicity of potassium-modified acid–base bifunctional SBA-15 on the aldol condensation of furfural and acetone. Our results demonstrate the crucial role of potassium loading in the interaction with bifunctional 12MgAl-SBA-15, and how it can improve the basicity of the material to achieve high furfural conversion under mild reaction conditions. However, high potassium loading can cause blockage of the mesopore structure and hinder accessibility to the acid sites of the material. Despite this limitation, the mesoporous SBA-15 exhibits considerable recyclability of up to four cycles when it is regenerated through open-air calcination. More crucially, these preliminary results meaningfully enlighten us on designing non-interfering strong acid–base active sites in SBA-15 for one-pot transformation of furfural and acetone to advanced jet-fuel ranged alkanes or petrochemical diols, which take place *via* cascade aldol condensation and hydrodeoxygenation processes. We are currently examining the activity of the developed potassium-modified bifunctional acid–base MgAl-SBA-15 in one-pot transformation of furfural and acetone using a high-pressure and temperature reactor system.

Conflicts of interest

There are no conflicts to declare.

Acknowledgements

The authors thank European Structural and Investment Funds, OP RDE-funded project 'ChemJets2' (CZ.02.2.69/0.0/0.0/18_053/0016974) for its financial support. Mahashanon Arumugam and Amin Osatiashtiani would like to thank Aston University for the International Visiting Scholar Fund.

References

1 V. Aristizábal and Á. Gómez, Biorefineries based on coffee cut-stems and sugarcane bagasse: Furan-based compounds and alkanes as interesting products, *Bioresour. Technol.*, 2015, **196**, 480–489.
2 Y. S. Jang, B. Kim, J. H. Shin, Y. J. Choi, S. Choi, C. W. Song, J. Lee, H. G. Park and S. Y. Lee, Bio-based production of C_2–C_6 platform chemicals, *Biotechnol. Bioeng.*, 2012, **109**, 2437–2459.
3 H. Li, S. Yang, S. Saravanamurugan and A. Riisager, Glucose isomerization by enzymes and chemo-catalysts: status and current advances, *ACS Catal.*, 2017, **7**, 3010–3029.
4 A. Eisentraut, *Sustainable Production of Second-Generation Biofuels: Potential and Perspectives in Major Economies and Developing Countries*, 2010.
5 H. Li, A. Riisager, S. Saravanamurugan, A. Pandey, R. S. Sangwan, S. Yang and R. Luque, Carbon-increasing catalytic strategies for upgrading biomass into energy-intensive fuels and chemicals, *ACS Catal.*, 2018, **8**, 148–187.
6 A. Deneyer, T. Ennaert and B. F. Sels, Straightforward sustainability assessment of sugar-derived molecules from first-generation biomass, *Curr. Opin. Green Sustainable Chem.*, 2018, **10**, 11–20.
7 B. G. Harvey and H. A. Meylemans, The role of butanol in the development of sustainable fuel technologies, *J. Chem. Technol. Biotechnol.*, 2011, **86**, 2–9.
8 C. Barrett, J. Chheda, G. Huber and J. Dumesic, Single-reactor process for sequential aldol-condensation and hydrogenation of biomass-derived compounds in water, *Appl. Catal., B*, 2006, **66**, 111–118.
9 A. Ndou, N. Plint and N. Coville, Dimerisation of ethanol to butanol over solid-base catalysts, *Appl. Catal., A*, 2003, **251**, 337–345.
10 P. A. Zapata, J. Faria, M. Pilar Ruiz and D. E. Resasco, Condensation/hydrogenation of biomass-derived oxygenates in water/oil emulsions stabilized by nanohybrid catalysts, *Top. Catal.*, 2012, **55**, 38–52.
11 W. Shen, G. A. Tompsett, K. D. Hammond, R. Xing, F. Dogan, C. P. Grey, W. C. Conner Jr, S. M. Auerbach and G. W. Huber, Liquid phase aldol condensation reactions with MgO-ZrO_2 and shape-selective nitrogen-substituted NaY, *Appl. Catal., A*, 2011, **392**, 57–68.
12 O. Kikhtyanin, V. Korolova, A. Spencer, L. Dubnová, B. Shumeiko and D. Kubička, On the influence of acidic admixtures in furfural on the performance of MgAl mixed oxide catalysts in aldol condensation of furfural and acetone, *Catal. Today*, 2021, **367**, 248–257.
13 L. Dubnová, L. Smolakova, O. Kikhtyanin, J. Kocik, D. Kubička, M. Zvolská, M. Pouzar and L. Čapek, The role of ZnO in the catalytic behaviour of Zn-Al mixed oxides in aldol condensation of furfural with acetone, *Catal. Today*, 2021, **379**, 181–191.

Open Access Article. Published on 31 May 2023. Downloaded on 12/4/2025 5:24:02 PM.
This article is licensed under a Creative Commons Attribution 3.0 Unported Licence.

14 O. Kikhtyanin, L. Čapek, Z. Tišler, R. Velvarská, A. Panasewicz, P. Diblíková and D. Kubička, Physicochemical properties of MgGa mixed oxides and reconstructed layered double hydroxides and their performance in aldol condensation of furfural and acetone, *Front. Chem.*, 2018, **6**, 176.

15 L. Hora, V. Kelbichová, O. Kikhtyanin, O. Bortnovskiy and D. Kubička, Aldol condensation of furfural and acetone over MgAl layered double hydroxides and mixed oxides, *Catal. Today*, 2014, **223**, 138–147.

16 V. Korolova, O. Kikhtyanin, F. Ruiz-Zepeda, M. Lhotka, M. Veselý and D. Kubička, Fading memory of MgAl hydrotalcites at mild rehydration conditions deteriorates their performance in aldol condensation, *Appl. Catal., A*, 2022, **632**, 118482.

17 D. P. Debecker, E. M. Gaigneaux and G. Busca, Exploring, tuning, and exploiting the basicity of hydrotalcites for applications in heterogeneous catalysis, *Chem.–Eur. J.*, 2009, **15**, 3920–3935.

18 C. Xu, Y. Gao, X. Liu, R. Xin and Z. Wang, Hydrotalcite reconstructed by *in situ* rehydration as a highly active solid base catalyst and its application in aldol condensations, *RSC Adv.*, 2013, **3**, 793–801.

19 S. Abelló, D. Vijaya-Shankar and J. Pérez-Ramírez, Stability, reutilization, and scalability of activated hydrotalcites in aldol condensation, *Appl. Catal., A*, 2008, **342**, 119–125.

20 O. Kikhtyanin, V. Kelbichová, D. Vitvarová, M. Kubů and D. Kubička, Aldol condensation of furfural and acetone on zeolites, *Catal. Today*, 2014, **227**, 154–162.

21 F. A. Carey and R. J. Sundberg, *Advanced Organic Chemistry: Part A: Structure and Mechanisms*, Springer Science & Business Media, 2007.

22 N. Liu, Z. Wu, M. Li, S. Li, Y. Li, R. Yu, L. Pan and Y. Liu, A novel strategy for constructing mesoporous solid superbase catalysts: bimetallic Al–La oxides supported on SBA-15 modified with KF, *Catal. Sci. Technol.*, 2017, **7**, 725–733.

23 J. Zhu, D. Chen, Z. Wang, Q. Wu, Z. Yin and Z. Wei, Synthesis of glycerol carbonate from glycerol and dimethyl carbonate over CaO-SBA-15 catalyst, *Chem. Eng. Sci.*, 2022, **258**, 117760.

24 W. Zheng, X. Kan, F. Liu, H. Li, F. Song, G. Xia, J. Liu and F. Liu, Ordered Mesoporous Carbon Encapsulating KF: Efficient and Stable Solid Base for Biodiesel and Fine Chemical Catalytic Synthesis, *ACS Sustainable Chem. Eng.*, 2022, **10**, 3477–3487.

25 K. R. Kloetstra and H. van Bekkum, Base and acid catalysis by the alkali-containing MCM-41 mesoporous molecular sieve, *J. Chem. Soc., Chem. Commun.*, 1995, 1005–1006.

26 L. B. Sun, J. H. Kou, Y. Chun, J. Yang, F. N. Gu, Y. Wang, J. H. Zhu and Z. G. Zou, New attempt at directly generating superbasicity on mesoporous silica SBA-15, *Inorg. Chem.*, 2008, **47**, 4199–4208.

27 Z. Y. Wu, Q. Jiang, Y. M. Wang, H. J. Wang, L. B. Sun, L. Y. Shi, J. H. Xu, Y. Wang, Y. Chun and J. H. Zhu, Generating superbasic sites on mesoporous silica SBA-15, *Chem. Mater.*, 2006, **18**, 4600–4608.

28 W. Trisunaryanti, E. Suarsih and I. I. Falah, Well-dispersed nickel nanoparticles on the external and internal surfaces of SBA-15 for hydrocracking of pyrolyzed α-cellulose, *RSC Adv.*, 2019, **9**, 1230–1237.

29 S. Karthikeyan, M. Pachamuthu, M. A. Isaacs, S. Kumar, A. F. Lee and G. Sekaran, Cu and Fe oxides dispersed on SBA-15: a Fenton type bimetallic catalyst for *N*,*N*-diethyl-*p*-phenyl diamine degradation, *Appl. Catal., B*, 2016, **199**, 323–330.

30 J. Wang, H. Ge and W. Bao, Synthesis and characteristics of SBA-15 with thick pore wall and high hydrothermal stability, *Mater. Lett.*, 2015, **145**, 312–315.

31 J. C. Manayil, A. Osatiashtiani, A. Mendoza, C. M. Parlett, M. A. Isaacs, L. J. Durndell, C. Michailof, E. Heracleous, A. Lappas and A. F. Lee, Impact of macroporosity on catalytic upgrading of fast pyrolysis bio-oil by esterification over silica sulfonic acids, *ChemSusChem*, 2017, **10**, 3506–3511.

32 Y. Zhang, Y. Chen, J. Pan, M. Liu, P. Jin and Y. Yan, Synthesis and evaluation of acid–base bi-functionalized SBA-15 catalyst for biomass energy conversation, *Chem. Eng. J.*, 2017, **313**, 1593–1606.

33 S. Jiang, S. Ding, Q. Jiang, Y. Zhou, S. Yuan, X. Geng, G. Yang and C. Zhang, Effects of Al introduction methods for Al-SBA-15 on NiMoS active phase morphology and hydrodesulfurization reaction selectivities, *Fuel*, 2022, **330**, 125493.

34 M. Pandey, D. Jadav, A. Manhas, S. Kediya, N. Tsunoji, R. Kumar, S. Das and M. Bandyopadhyay, Synthesis and characterization of mononuclear Zn complex, immobilized on ordered mesoporous silica and their tunable catalytic properties, *Mol. Catal.*, 2022, **525**, 112365.

35 V. K. Tomer, R. Malik, S. Jangra, S. Nehra and S. Duhan, One pot direct synthesis of mesoporous SnO_2/SBA-15 nanocomposite by the hydrothermal method, *Mater. Lett.*, 2014, **132**, 228–230.

36 J. Colmenares-Zerpa, J. Gajardo, A. Peixoto, D. Silva, J. Silva, F. Gispert-Guirado, J. Llorca, E. Urquieta-Gonzalez, J. Santos and R. Chimentão, High zirconium loads in Zr-SBA-15 mesoporous materials prepared by direct-synthesis and pH-adjusting approaches, *J. Solid State Chem.*, 2022, 123296.

37 N. Aider, A. Smuszkiewicz, E. Pérez-Mayoral, E. Soriano, R. M. Martín-Aranda, D. Halliche and S. Menad, Amino-grafted SBA-15 material as dual acid–base catalyst for the synthesis of coumarin derivatives, *Catal. Today*, 2014, **227**, 215–222.

38 L. Shi, Y. Wang, A. Ji, L. Gao and Y. Wang, *In situ* direct bifunctionalization of mesoporous silica SBA-15, *J. Mater. Chem.*, 2005, **15**, 1392–1396.

39 M. A. Isaacs, C. Parlett, N. Robinson, L. J. Durndell, J. C. Manayil, S. K. Beaumont, S. Jiang, N. S. Hondow, A. C. Lamb and D. Jampaiah, A spatially orthogonal hierarchically porous acid–base catalyst for cascade and antagonistic reactions, *Nat. Catal.*, 2020, **3**, 921–931.

40 R. Ramos, J. M. Hidalgo, M. Göpel, Z. Tišler, F. Bertella, A. Martínez, O. Kikhtyanin and D. Kubička, Catalytic conversion of furfural-acetone condensation products into

Open Access Article. Published on 31 May 2023. Downloaded on 12/4/2025 5:24:02 PM.
This article is licensed under a Creative Commons Attribution 3.0 Unported Licence.

bio-derived C8 linear alcohols over NiCu/Al-SBA-15, *Catal. Commun.*, 2018, **114**, 42–45.

41 R. Ramos, Z. Tišler, O. Kikhtyanin and D. Kubička, Towards understanding the hydrodeoxygenation pathways of furfural–acetone aldol condensation products over supported Pt catalysts, *Catal. Sci. Technol.*, 2016, **6**, 1829–1841.

42 W. Farneth and R. Gorte, Methods for characterizing zeolite acidity, *Chem. Rev.*, 1995, **95**, 615–635.

43 C. Yu, B. Tian, J. Fan, G. D. Stucky and D. Zhao, Nonionic block copolymer synthesis of large-pore cubic mesoporous single crystals by use of inorganic salts, *J. Am. Chem. Soc.*, 2002, **124**, 4556–4557.

44 Y. M. Wang, Z. Y. Wu, L. Y. Shi and J. H. Zhu, Rapid functionalization of mesoporous materials: directly dispersing metal oxides into as-prepared SBA-15 occluded with template, *Adv. Mater.*, 2005, **17**, 323–327.

45 J. Tittensor, R. Gorte and D. Chapman, Isopropylamine adsorption for the characterization of acid sites in silica-alumina catalysts, *J. Catal.*, 1992, **138**, 714–720.

46 J. Zhao, J. Xie, C.-T. Au and S.-F. Yin, One-pot synthesis of potassium-loaded MgAl oxide as solid superbase catalyst for Knoevenagel condensation, *Appl. Catal., A*, 2013, **467**, 33–37.

47 O. Kikhtyanin, R. Bulánek, K. Frolich, J. Čejka and D. Kubička, Aldol condensation of furfural with acetone over ion-exchanged and impregnated potassium BEA zeolites, *J. Mol. Catal. A: Chem.*, 2016, **424**, 358–368.

48 D. Yang, G. Wang, H. Wu, X. Guo, S. Zhang, Z. Li and C. Li, Deactivation behavior on VPO and VPO-Zr catalysts in the aldol condensation of methyl acetate and formaldehyde, *Catal. Today*, 2018, **316**, 122–128.

49 F. Kleitz, W. Schmidt and F. Schüth, Calcination behavior of different surfactant-templated mesostructured silica materials, *Microporous Mesoporous Mater.*, 2003, **65**, 1–29.